Dissolution at a Ductile Crack Tip

Wenjia Gu and Derek H. Warner*
Cornell Fracture Group, School of Civil and Environmental Engineering, Cornell University, Ithaca, New York 14850, USA

(Received 7 April 2021; revised 30 August 2021; accepted 1 September 2021; published 30 September 2021)

The growth of cracks can be substantially influenced by the environment. Atomic modeling provides a means to isolate the action of individual mechanisms involved in such complex processes. Here, we utilize a newly implemented multiscale modeling approach to assess the role of material dissolution on long crack growth in a ductile material. While we find dissolution to be capable of freeing arrested fatigue cracks, the crack tip is always blunted under both static and cyclic loading, suggesting that dissolution has an overall crack arresting effect. Despite observations of plasticity-induced-dissolution and dissolution-induced-plasticity that are consistent with macroscale experiments, dissolution-induced-blunting is found to be independent of mechanical loading magnitude. This will simplify implementation of the dissolution-induced-blunting process into continuum crack growth models.

DOI: 10.1103/PhysRevLett.127.146001

The environment can accelerate crack growth rates by orders of magnitude, leading to unexpected and catastrophic outcomes. Examples include the role of humidity on aerospace alloys [1,2], sulfides on pipeline steels [3], and liquid metals on reactor pressure vessels [4]. Yet, there are instances where environment acts in the opposite way, improving structural performance; with examples ranging from structural metals in specific liquid environments [5–10] to the dissolving action of osteoclasts on bone, which is essential for maintaining bone fracture resistance [11].

Despite a long documented history of environmental effects [12], an understanding of the controlling mechanisms remain clouded. At fault are several challenges. First, multiple mechanisms can act simultaneously, e.g., dissolution, oxide fracture, oxide formation, material redeposition, and hydrogen embrittlement. Second, the scale of the material separation process on which the environment acts is atomistic, inhibiting direct observation [1,13–18]. In light of these challenges, atomistic modeling can serve as a powerful probe to illuminate the mechanisms governing environmental effects [19], providing a means to study the material separation processes under the action of isolated mechanisms. Here, the focus is directed towards the action of material dissolution at the tip of a long and intrinsically ductile crack. Upon increasing load, an intrinsically ductile crack will first emit dislocations from its tip, plastically blunting as opposed to cleaving [20,21]; and, a "long" crack will exhibit behavior that is independent of its length when the stress intensity factor is held constant [22].

A novel implementation of the concurrently coupled atomistic-discrete dislocation approach [23] is harnessed to allow the study of a highly deformed crack tip in a well-developed crack stress field, better approaching real-world conditions. The model consists of an edge crack centered in a [4464b x 4464b] square domain (Fig. S1 [24]), which is created by removing 3 consecutive planes of atoms. The [268b x 134b] atomistic region at the crack tip is coupled to the surrounding continuum region by self-consistent displacement boundary conditions [25]. Mechanical equilibrium is obtained using LAMMPS [26] for the atomistic region and FEniCS [27] for the continuum region. We refer to this approach as LF-CADD. The continuum region is governed by 2D plane-strain linear elasticity with elastic constants chosen to match the interatomic potential of the atomistic region.

Loads are applied by prescribed displacements at the outer boundary of the continuum region corresponding to the solution for a sharp crack in a linear elastic isotropic material subjected to mode I loading. The prescribed displacement is a function of the current crack tip position to avoid artificially inhibiting crack growth. The loading increment after each mechanical equilibration was $0.015/K_I^{\mathrm{nuc}}$. K_I^{nuc} represents the mode I stress intensity factor at which the first dislocation nucleates from the crack tip under ramped loading. For the interatomic potential and crack-crystal orientation that was simulated, K_I^{nuc} corresponds to a full edge dislocation on the close packed plane inclined at 60° from the crack plane. All cyclic loading simulations had a constant stress intensity range $[\Delta K^* = (K_I^{\mathrm{max}} - K_I^{\mathrm{min}})/K_I^{\mathrm{nuc}}]$ throughout the simulation with a load ratio ($R = K_I^{\mathrm{min}}/K_I^{\mathrm{max}}$) of 0.25.

Even with the multiscale approach and the utilization of substantial computational resources, gaps between the atomistic model and reality still exist. Accordingly, the atomistic study must be focused towards specific features. Here, we target the large deformation history associated with cyclic loading to hundreds of cycles; motivated by the little understood but technologically consequential process

of corrosion fatigue, which can induce catastrophic failure under loads and environments that would be benign if acting alone [28,29].

The high cycle counts are achieved by simulating a 2D hexagonal lattice in the athermal limit. The response of the hexagonal lattice is governed by the intrinsically ductile interatomic potential of Rajan *et al.* (potential A in Ref. [30]). This approach is appealing in that it offers three dislocation slip systems and glissile dislocation reactions in two dimensions. In contrast, the alternative of using thin 3D crystallographies overconstrains plastic slip relative to real 3D geometries [31–34].

An additional strategy to make the many cycle simulations tractable is to limit the size of the plastic zone, reducing the need to integrate the motion of many dislocations over long distances during each load cycle. Towards this goal, we investigated the role of dislocation glide resistance in the continuum domain [35], whereby greater glide resistances reduce the plastic zone size making the simulations less computationally demanding. Examining a wide range of glide resistances, fatigue crack growth is observed to be independent of this parameter [36]. This result is consistent with the conclusion of discrete dislocation continuum modeling [37,38] and experiments [6,38–43] that have shown dislocation glide resistance to not directly influence near threshold fatigue crack growth. The result provides validity for subsequently presented simulations where dislocation motion was constrained to the atomistic domain (effectively imposing a high glide resistance) in order to access high cycle counts.

For simplicity and consistency with the athermal limit approximation, dissolution was modeled by the removal of the highest energy surface atom followed by mechanical equilibration. In other terms, the simulation cell modeled a region undergoing material dissolution (e.g., an anode), with the most weakly bound atom being removed from the simulation cell. Surface diffusion and material redeposition (the reverse reaction) were not modeled. The atom removal-mechanical equilibration process was repeated to simulate progressive dissolution in the context of the mechanical equilibration timescale being short relative to the interval between single atom dissolution events. The sensitivity of the subsequently presented results to this approach was investigated by performing a second set of simulations where atom removal was random. In this case, the probability of removing a particular surface atom "i" was chosen to be proportional to e^{E_i/k_BT}, where E_i represents the energy of a surface atom i and k_BT was set to 0.0257, corresponding to room temperature. The results of the simulations with random surface atom removal did not qualitatively differ from those presented here.

To begin, the response of long cracks subjected to dissolution at fixed stress intensity factors is presented. A representative case at a fixed loading of $K^* = K_I/K_I^{\mathrm{nuc}} = 1.96$ is shown in Fig. 1. The images depict a progressive crack opening process due to dissolution, which is the first key result of this Letter. In coloring atoms by their energy levels, Fig. 1 illustrates that the effect of the crack tip stress field is overwhelmed by the differences in the atomic coordination number of surface atoms. In most cases, dissolution begins with the removal

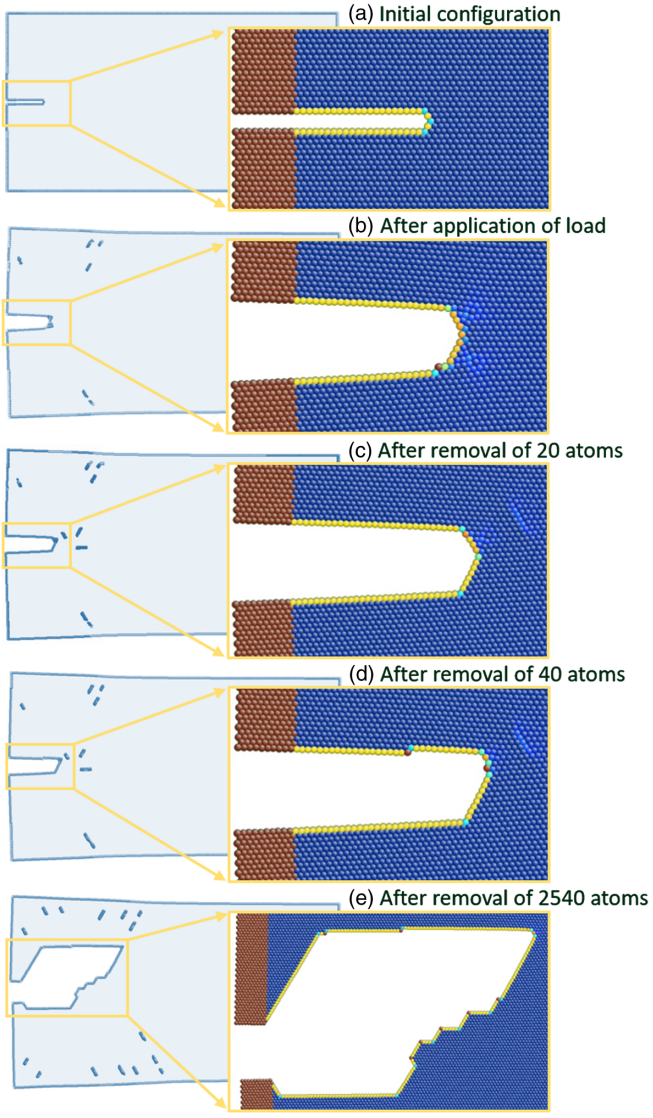

FIG. 1. Atomistic domain and crack tip under static loading with dissolution. Only atoms with a centrosymmetry parameter not equal to that of the perfect hexagonal crystal are shown in the left figures, i.e., atoms at the crack surface, continuum-atomistic interface, and dislocation cores. Figures on the right show zoomed views of the crack with atoms colored by their energy, with the exception of the continuum region pad atoms that are shown in red. (a) Initial configuration at $K^* = 0.0$; (b) after application of load before atom removal ($K^* = 1.96$); (c) after removal of 20 atoms ($K^* = 1.96$); (d) after removal of 40 atoms ($K^* = 1.96$); (e) after removal of 2540 atoms ($K^* = 1.96$).

of the lowly coordinated atoms at surface steps created by dislocation emission during mechanical loading. In the cases where no lowly coordinated atomic steps exist, the stress field does influence dissolution with atom removal occurring near a sharp corner of the crack. In this case a lowly coordinate surface step is formed and becomes the site for subsequent dissolution. Dissolution at surface steps does not lead to their removal, but causes step propagation, as can be seen in Fig. 1(d). Geometry dictates that a propagating step will either be absorbed into a corner of the crack tip or eventually propagate away from the crack tip, acting to open (blunt) the crack.

The dissolution of atoms at a loaded crack tip can cause load redistribution of sufficient magnitude to induce dislocation emission, as seen when comparing Fig. 1(c) with Fig. 1(b). In laboratory experiment, such bursts of dislocation emission due to dissolution may be detectable via acoustic emission. Relative to the vast literature on environmentally induced plasticity [29,44–47], this result is noteworthy in that it shows the induction of plasticity without a change in surface energy, surface step energy, or surface film structure. While dissolution is not focused at the crack tip, the resulting dislocation emission is most prevalent at the crack tip due to the load redistribution being most significant at that location. Subsequently, surface step formation occurs most frequently at the crack tip. However, the generation of surface steps at the crack tip does not sufficiently focus subsequent dissolution to the crack tip (such that crack growth dominates blunting) due to the propagation of the surface steps away from the crack tip.

On the whole, these simulations together with the long-established laboratory trend of plasticity induced dissolution [48,49] suggest that dissolution induced crack propagation (if it exists) must occur via a mechanism not included here, such as surface film rupture or heterogeneous phases [29,46,47,50,51].

Next, the results of simulations that examine the action of dissolution under cyclic mechanical loading are presented, i.e., fatigue loading. To provide a baseline for comparison, cyclic loading simulations without dissolution were also performed. The progression of crack geometry without dissolution is shown in Fig. 3(a). From these curves it is clear that the crack arrests after an initial growth stage, with all dislocation activity becoming fully reversible over the course of the loading cycle (Supplemental Material, Fig. S2 [24]). As discussed in Ref. [36], this result is not thought to be attributable to simulation artifacts, but instead result from the inaction of the mechanisms required for fatigue crack growth in vacuum. As such, we consider the loadings to be below the vacuum fatigue crack growth threshold.

Similar to the static loading simulations, dissolution was simulated by successively removing the highest energy atoms then mechanically equilibrating at the peak of each loading cycle. Comparing simulations with and without dissolution, the dissolution processes unlocks cracks from arrested states. In this way the dissolution process is found to be capable of promoting crack growth under cyclic mechanical loading, which is the second key result of this Letter.

A detailed example of this process is shown in Fig. 2 for $\Delta K^* = 1.47$ and a dissolution rate of 10 atoms per mechanical loading cycle. The crack arrests at cycle 78 as emitted dislocations during loading are absorbed back to the crack during unloading, resulting in a reversible state. In cycle 83, the dissolution process is solely focused on a surface step at the crack face away from where dislocation emission and absorption occur. As such, the crack remains in the arrested state. However, in cycle 84, the propagating surface step is absorbed into the boundary of the atomistic domain. Subsequent dissolution then occurs at the corners of the crack tip, causing a redistribution of load that is sufficient to induce dislocation emission. Ultimately, the action of dissolution and the induced dislocation emission advance the position of the crack tip at the peak of the next loading cycle, unlocking the crack from its reversible arrested state.

Increasing the per cycle dissolution rate decreases the time between crack tip atom removal events. This shortens the time that a crack resides in arrested states, which can consequently increase the average crack growth rate. The behavior is shown in Figs. 3(g) and 3(i), which display the results of simulations at $\Delta K^* = 1.47$ with differing dissolution rates. The enhancement of crack growth with dissolution plateaus, in correspondence with the elimination of arrested states to be unlocked. On this point, arrested states are less common at higher cyclic loading amplitudes, e.g., $\Delta K^* = 2.21$; and thus, the enhancement offered by dissolution is saturated to a lower value of dissolution rate [Figs. 3(d) and 3(f)].

An increase in the dissolution rate also accelerates the rate of atom removal at the crack faces through increased surface step propagation. As in the static loading case, increasing the dissolution rate increases the crack opening under cyclic loading [Figs. 3(e) and 3(h)]. Consistent with the process not depending on the number of surface steps (but the collective distance that steps have propagated), the relationship between crack opening and dissolution rate is found to be linear and insensitive to loading amplitude [Figs. 3(c),3(f), and 3(i)]. Also consistent with the process not depending on the number of surface steps is the insensitivity of the simulation results to the randomness of the surface atom removal procedure mentioned earlier.

In total, the preceding indicates that while dissolution can enhance fatigue crack growth by freeing arrested cracks, dissolution will always enhance crack opening. Given the nature of crack tip stresses, this combination of actions is predicted to lead to crack arrest at real-world engineering scales (millimeter) [52]. Characterizing crack opening as crack tip radius, ρ, and acknowledging that this value is orders of magnitude less than the crack length a, Inglis's solution [53] gives near tip stresses that scale as

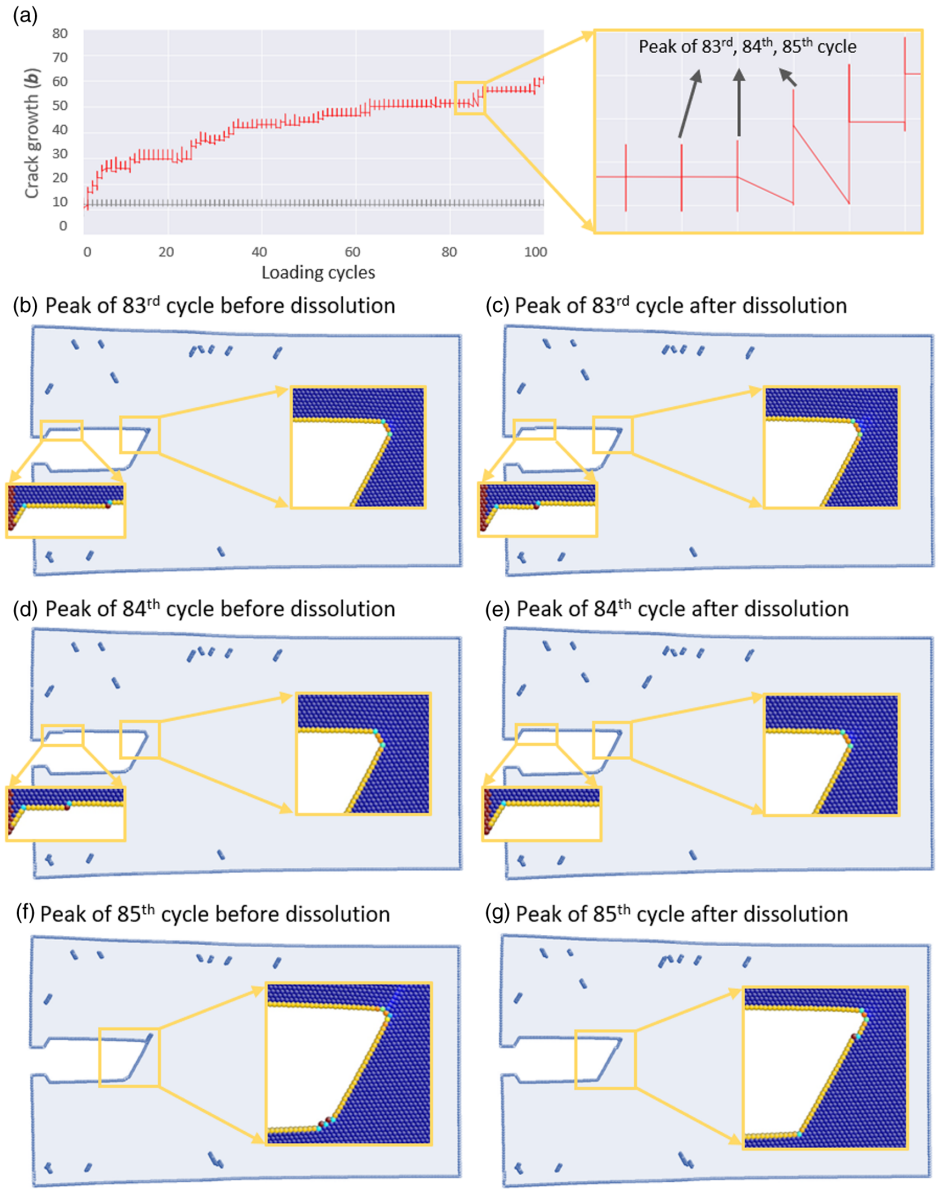

FIG. 2. Atomistic domain and crack tip in cyclic loading simulation ($\Delta K^* = 1.47$) with dissolution rate of 10 atoms/cycle. Only atoms with a centrosymmetry parameter not equal to that of the perfect hexagonal crystal are shown in the primary images, i.e., atoms at the crack surface, continuum-atomistic interface, and dislocation cores. Inset images give zoomed views with atoms colored by their energy. (a) Crack growth in the x direction as a function of loading cycles with (in red) and without (in gray) dissolution; (b) peak of the 83rd cycle before dissolution; (c) peak of the 83rd cycle after dissolution; (d) peak of the 84th cycle before dissolution; (e) peak of the 84th cycle after dissolution; (f) peak of the 85th cycle before dissolution; (g) peak of the 85th cycle after dissolution.

$$\sigma_{\text{crack tip}} \propto \sqrt{\frac{a}{\rho}}. \tag{1}$$

$$\sigma_{\text{crack tip}} \propto \sqrt{\frac{a_0 + \Delta a}{\rho_0 + \Delta\rho}} \approx \sqrt{\frac{a_0}{\rho + \Delta\rho}}, \quad \text{when } \frac{a_0}{\Delta a} \gg \frac{\rho_0}{\Delta\rho}. \tag{2}$$

Considering (i) an initial crack with length $a = a_0$ and a crack tip radius $\rho = \rho_0$, (ii) an increment of dissolution that changes the crack dimensions by Δa and $\Delta\rho$, and (iii) a relative change in crack length that is much smaller than the relative change in crack tip radius, $a_0/\Delta a \gg \rho_0/\Delta\rho$, the near tip stresses scale as

Thus, while an increment in dissolution may result in a Δa and $\Delta\rho$ of different magnitudes, the dominance of the a_0 length scale implies a decrease in the crack tip stresses with dissolution. For example, a crack of $a_0 = 100$ μm and $\rho_0 = 1$ nm that undergoes 10 nm of dissolution induced advance

and opening would experience a decrease in near tip stresses of 70%.

In total, the results presented here predict that dissolution induces crack arrest via a dissolution induced opening (blunting) phenomenon, independent of any dissolution induced crack growth. This motivates the question of whether dissolution induced opening might eventually cease while dissolution induced crack growth remains active, which would ultimately equate to dissolution promoting crack growth at the engineering scale. The simulation results of Figs. 3(a)–3(c) which extend to 400 cycles do not show any indication of a trend towards this behavior; nonetheless, the results here do not preclude it.

The inhibition or even arrest of cracks due to environment has been widely observed in the laboratory. In some cases involving structural alloys in aqueous and liquid metal environments, the behavior has been attributed to crack blunting via dissolution [5–10]. However, in no cases could the dissolution mechanism be isolated from other potential mechanisms, e.g., the progressive buildup of corrosion products [54,55]. Thus, the modeling outcomes presented here together with the available experimental data support the assertion that dissolution can inhibit and even arrest crack growth (in the face of the observed dissolution induced plasticity and plasticity enhanced dissolution). As such, this work motivates the incorporation of dissolution blunting mechanisms into crack growth prognosis (as done by Ref. [8]), and suggests that such a mechanism can be included in a load independent formulation.

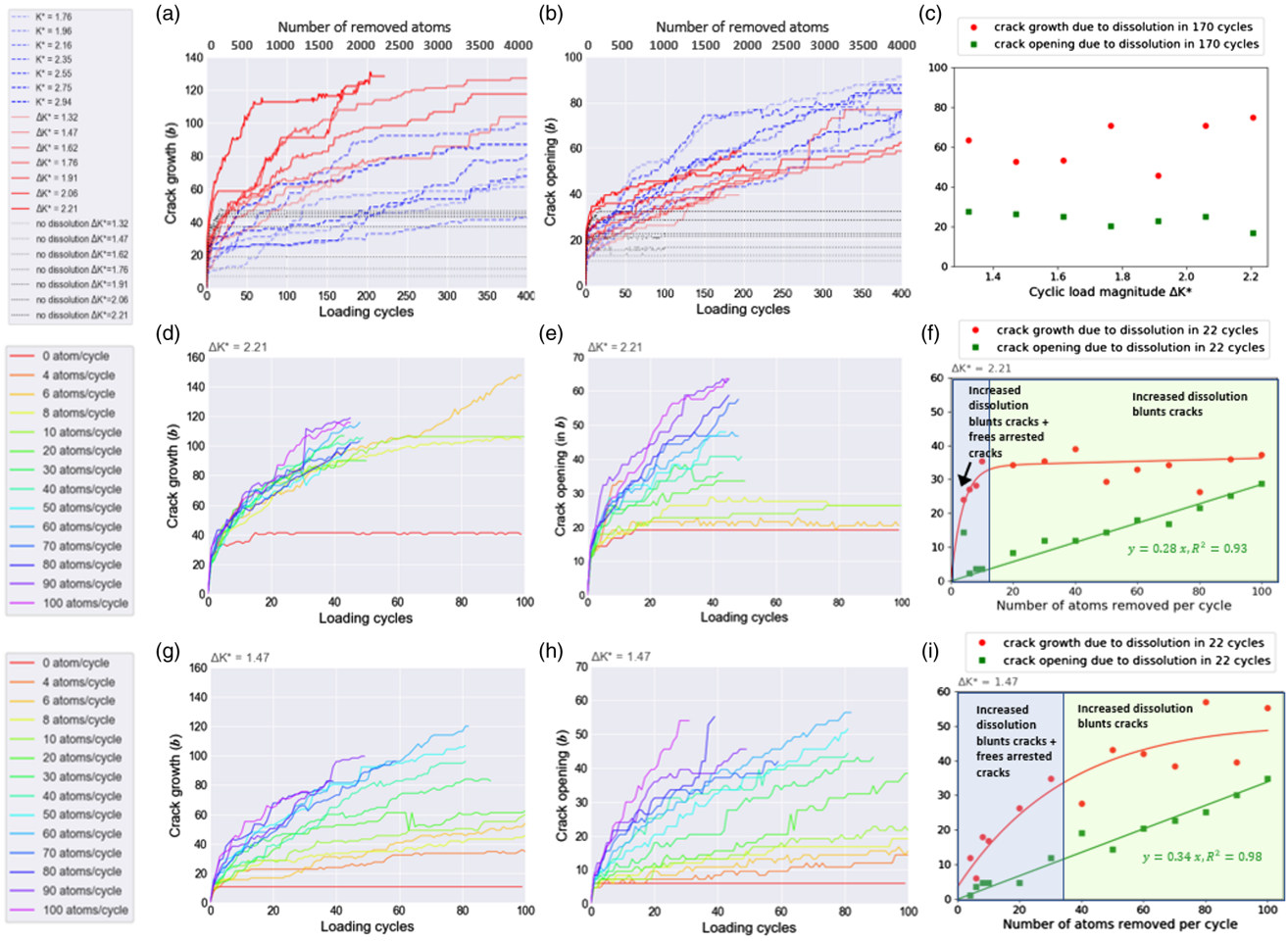

FIG. 3. Crack growth and opening for a range of loadings and dissolution rates. In (a) and (b) cyclically loaded simulations with dissolution of 10 atoms per cycle are compared to a corresponding set of simulations with no dissolution with respect to the number of loading cycles. These simulations are also compared to a corresponding set of statically loaded simulations with respect to the number of atoms removed due to dissolution. In (c) the dissolution enhanced crack growth and opening for the cyclically loaded simulations is shown to be independent of loading amplitude at 170 cycles. In (d) through (f), and (g) through (i) the effects of dissolution rate are shown for two cyclic loading amplitudes, i.e., $\Delta K^* = 2.21$ and $\Delta K^* = 1.47$, respectively. The units of the y axes are normalized by b. In (f) and (i) the gray region represents a regime where increasing dissolution rate will increase crack blunting and the frequency by which arrested cracks are freed. In the gray region, crack arrest is not common so increasing the dissolution rate will only increase crack blunting.

This work was supported by the Office of Naval Research (Grant No. N000141712035). The authors thank Mingjie Zhao for his contribution to the LF-CADD code development, and A. K. Vasudevan for inspiring us to perform dissolution-crack simulations.

*Corresponding author.
derek.warner@cornell.edu

[1] S. P. Lynch, Environmentally assisted cracking: Overview of evidence for an adsorption-induced localised-slip process, Acta Metall. **36**, 2639 (1988).
[2] J. T. Burns, R. W. Bush, J. H. Ai, J. L. Jones, Y. Lee, and R. P. Gangloff, Effect of water vapor pressure on fatigue crack growth in Al-Zn-Cu-Mg over wide-range stress intensity factor loading, Eng. Fract. Mech. **137**, 34 (2015).
[3] R. L. Eadie, K. E. Szklarz, and R. L. Sutherby, Corrosion fatigue and near-neutral pH stress corrosion cracking of pipeline steel and the effect of hydrogen sulfide, Corrosion **61**, 167 (2005).
[4] P. M. Scott and A. E. Truswell, Corrosion fatigue crack growth in reactor pressure vessel steels in PWR primary water, J. Pressure Vessel Technol. Trans. ASME **105**, 245 (1983).
[5] A. Creager and P. C. Paris, Elastic field equations for blunt cracks with reference to stress corrosion cracking, Int. J. Fract. Mech. **3**, 247 (1967).
[6] M. O. Speidel, M. J. Blackburn, T. R. Beck, and J. A. Feeney, Corrosion fatigue and stress corrosion crack growth in high strength aluminum alloys, magnesium alloys, and titanium alloys exposed to aqueous solutions, in *Corrosion Fatigue: Chemistry, Mechanics and Microstructure* (National Association of Corrosion Engineers, Huston, 1972), pp. 343–345.
[7] J. C. Radon, C. M. Branco, and L. E. Culver, Crack blunting and arrest in corrosion fatigue of mild steel, Int. J. Fract. **12**, 467 (1976).
[8] I. M. Austen, in *Quantitative Understanding of Corrosion Fatigue Crack Growth Behaviour* (Commission of the European Communities, Directorate-General Science, Research and Development, Brussels, 1983).
[9] D. A. Wheeler, R. G. Hoagland, and J. P. Hirth. Evidence for crack tip oxidation effects during the liquid metal embrittlement of AA 7075 aluminum alloy by mercury, Corrosion **45**, 207 (1989).
[10] P. J. L. Fernandes and D. R. H. Jones, The effect of temperature on fatigue crack growth in liquid metal environments, Corros. Sci. **38**, 745 (1996).
[11] J. F. Charles and A. O. Aliprantis, Osteoclasts: More than 'bone eaters', Trends Mol. Med. **20**, 449 (2014).
[12] Pliny the Elder, in *Natural History*, edited by A. Islip (Adam Islip, London, 1634).
[13] S. M. Ohr, An electron microscope study of crack tip deformation and its impact on the dislocation theory of fracture, Mater. Sci. Eng. **72**, 1 (1985).
[14] I. M. Robertson and H. K. Birnbaum, An HVEM study of hydrogen effects on the deformation and fracture of nickel, Acta Metall. **34**, 353 (1986).
[15] G. M. Bond, I. M. Robertson, and H. K. Birnbaum, The influence of hydrogen on deformation and fracture processes in high-strength aluminum alloys, Acta Metall. **35**, 2289 (1987).
[16] G. O. Ilevbare, O. Schneider, R. G. Kelly, and J. R. Scully, In situ confocal laser scanning microscopy of AA 2024-T3 corrosion metrology: I. Localized corrosion of particles *in situ* confocal laser scanning microscopy of AA 2024-T3 corrosion metrology, J. Electrochem. Soc. **151**, B453 (2004).
[17] A. Turnbull, Corrosion pitting and environmentally assisted small crack growth, Proc. R. Soc. A **470**, 20140254 (2014).
[18] T. J. Stannard, J. J. Williams, and S. S. Singh, 3d time-resolved observations of corrosion and corrosion-fatigue crack initiation and growth in peak-aged Al 7075 using synchrotron x-ray tomography, Corros. Sci. **138**, 340 (2018).
[19] E. Bitzek, J. R. Kermode, and P. Gumbsch, Atomistic aspects of fracture, Int. J. Fract. **191**, 13 (2015).
[20] James R. Rice, Dislocation nucleation from a crack tip: An analysis based on the Peierls concept, J. Mech. Phys. Solids **40**, 239 (1992).
[21] K. Tanaka and Y. Akiniwa, 4.06—modeling of fatigue crack growth: Mechanistic models, in *Comprehensive Structural Integrity*, edited by I. Milne, R. O. Ritchie, and B. Karihaloo (Pergamon, Oxford, 2003), pp. 165–189.
[22] S. Suresh, *Fracture Mechanics and Its Implications for Fatigue*, 2 ed. (Cambridge University Press, Cambridge, England, 1998).
[23] L. E. Shilkrot, R. E. Miller, and W. A. Curtin, Multiscale plasticity modeling: Coupled atomistics and discrete dislocation mechanics, J. Mech. Phys. Solids **52**, 755 (2004).
[24] See Supplemental Material at http://link.aps.org/supplemental/10.1103/PhysRevLett.127.146001 for simulation setup and results with reversible dislocation activity.
[25] R. E. Miller and E. B. Tadmor, A unified framework and performance benchmark of fourteen multiscale atomistic/aontinuum coupling methods, Model. Simul. Mater. Sci. Eng. **17**, 053001 (2009).
[26] S. Plimpton, Fast parallel algorithms for short-range molecular dynamics, J. Comput. Phys. **117**, 1 (1995).
[27] A. Logg, K. A. Mardal, and G. N. Wells, *Automated Solution of Differential Equations by the Finite Element Method*, Vol. 84 (Springer-Verlag, Berlin Heidelberg, 2012).
[28] S. Suresh, *Fatigue of Materials* (Cambridge University Press, Cambridge, England, 1998).
[29] R. P. Gangloff, in *Corrosion Fatigue Crack Propagation in Metals* (National Aeronautics and Space Administration, Washington, D.C., 1990), pp. 55–109.
[30] V. P. Rajan, D. H. Warner, and W. A. Curtin, An interatomic pair potential with tunable intrinsic ductility, Model. Simul. Mater. Sci. Eng. **24**, 025005 (2016).
[31] D. H. Warner, W. A. Curtin, and S. Qu, Rate dependence of crack-tip processes predicts twinning trends in f.c.c. metals, Nat. Mater. **6**, 876 (2007).
[32] G. Venkatramani, S. Ghosh, and M. Mills, A size-dependent crystal plasticity finite-element model for creep and load shedding in polycrystalline titanium alloys, Acta Mater. **55**, 3971 (2007).

[33] V. I. Yamakov, D. H. Warner, R. J. Zamora, E. Saether, W. A. Curtin, and E. H. Glaessgen, Investigation of crack tip dislocation emission in aluminum using multiscale molecular dynamics simulation and continuum modeling, J. Mech. Phys. Solids **65**, 35 (2014).

[34] Z. Fan, O. Hardouin Duparc, and M. Sauzay, Molecular dynamics simulation of surface step reconstruction and irreversibility under cyclic loading, Acta Mater. **102**, 149 (2016).

[35] The discontinuity of glide resistance between the atomistic and continuum domain is inconsequential for the results presented here as the driving force on dislocations in the atomistic domain is well above the glide resistance of ordinary engineering alloys.

[36] M Zhao, W Gu, and D. H. Warner, Atomic mechanism of near threshold fatigue crack growth in vacuum (to be published).

[37] R. Pippan, Dislocation emission and fatigue crack growth threshold, Acta Metall. Mater., **39**, 255 (1991).

[38] V. S. Deshpande, A. Needleman, and E. Van der Giessen, Scaling of discrete dislocation predictions for near-threshold fatigue crack growth, Acta Mater. **51**, 4637 (2003).

[39] A. J. McEVILY, Jr. and T. L. Johnston, The role of cross-slip in brittle fracture and fatige, Int. J. Fract. Mech. **3**, 45 (1967).

[40] P. K. Liaw, T. R. Lea, and W. A. Logsdon, Near-threshold fatigue crack growth behavior in metals, Acta Metal. **31**, 1581 (1983).

[41] R. Pippan, The effective threshold of fatigue crack propagation in aluminium alloys. I. The influence of yield stress and chemical composition, Philos. Mag. A **77**, 861 (1998).

[42] J. Wasén and E. Heier, Fatigue crack growth thresholds—The influence of Young's modulus and fracture surface roughness, International Journal of Fatigue **20**, 737 (1998).

[43] U. Zerbst, M. Vormwald, R. Pippan, H. P. Gänser, C. Sarrazin-Baudoux, and M. Madia, About the fatigue crack propagation threshold of metals as a design criterion—A review, Eng. Fract. Mech. **153**, 190 (2016).

[44] E. N. da C Andrade, The Rehbinder effect, Proc. Phys. Soc. **63**, 990 (1950).

[45] S. P. Lynch, The mechanism of liquid-metal embrittlement-crack growth in aluminum single crystals and other metals in liquid-metal environments, Technical Report No. 102, Aeronautical Research Laboratories, 1977.

[46] S. J. Hudak, Jr., D. L. Davidson, and R. A. Page, The role of crack-tip deformation in corrosion fatigue crack growth, in *Embrittlement by the Localized Crack Environment* (Metallurgical Society of AIME, Warrendale, 1984), pp. 173–197.

[47] F. P. Ford, Status of research on environmentally assisted cracking in LWR pressure vessel steels, J. Pressure Vessel Technol. **110**, 113 (1988).

[48] T. P. Hoar and J. M. West, Mechano-chemical anodic dissolution, Nature (London) **181**, 835 (1958).

[49] T. P. Hoar and J. C. Scully, Mechanochemical anodic dissolution of austenitic stainless steel in hot chloride solution at controlled electrode potential mechanochemical anodic dissolution of austenitic stainless steel in hot chloride solution at controlled electrode potential, J. Electrochem. Soc. **111**, 348 (1964).

[50] J. C. Scully, The mechanical parameters of stress-corrosion cracking, Corros. Sci. **8**, 759 (1968).

[51] R. W. Revie and H. H. Uhlig, *Corrosion and Corrosion Control* (John Wiley & Sons, New York, 2008).

[52] M. E. Hoffman and P. C. Hoffman, Corrosion and fatigue research—Structural issues and relevance to naval aviation, International Journal of Fatigue **23**, 1 (2001).

[53] C. E. Inglis, Stresses in a plate due to the presence of cracks and sharp cornersX, Trans. Inst. Naval Archit. **55**, 219 (1913).

[54] G. E. Nordmark and W. G. Fricke, Fatigue crack arrest at low stress intensities in a corrosive environment, Journal of Testing and Evaluation **6**, 301 (1978).

[55] R. van der Velden, H. L. Ewalds, W. A. Schultze, and A. Punter, Anomalous fatigue crack growth retardation in steels for offshore applications, in *Corrosion Fatigue: Mechanics, Metallurgy, Electrochemistry, and Engineering* (ASTM International, West Conshohocken, 1983), pp. 64–80.